

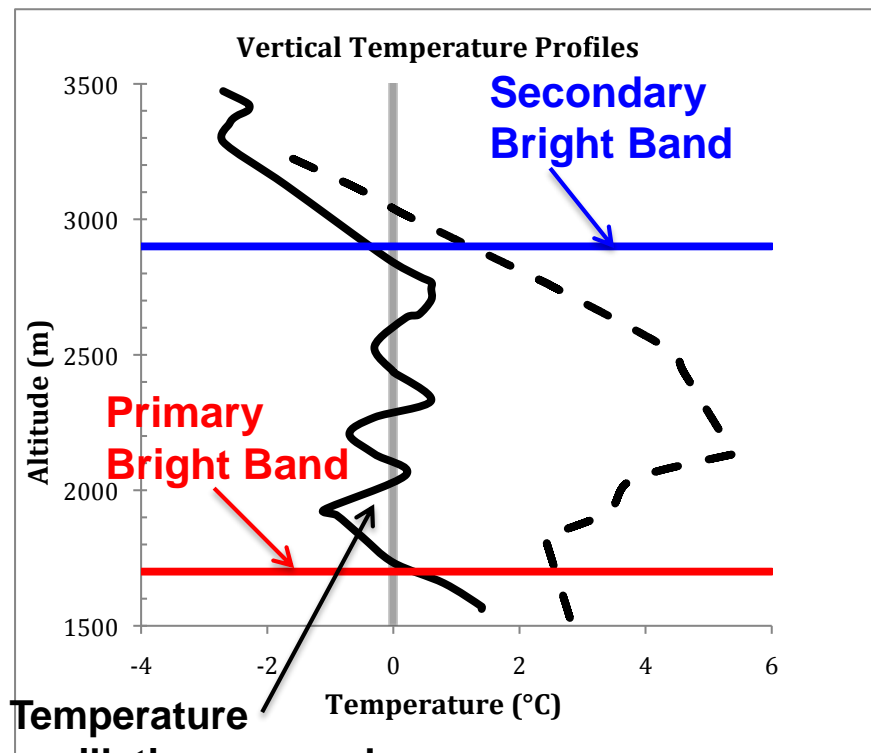
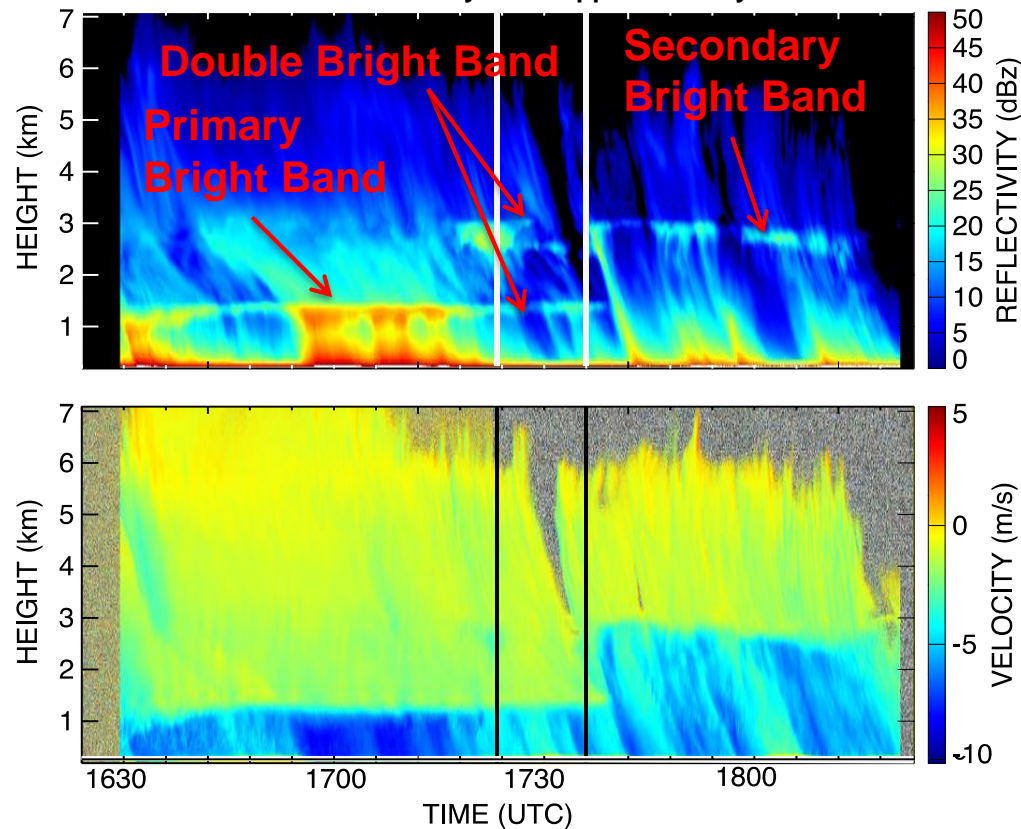


High-Resolution Vertical Observations of Double Bright Band Phenomenon

A. Emory¹, B. Demoz², K. Vermeesch², and M. Hicks³

¹Code 612, NASA/GSFC, ²JCET UMBC, ³NWS, Sterling, VA

Vertical Profiles of Reflectivity and Doppler Velocity from EDOP radar



Temperature oscillations around freezing level produce double bright band

11 May 2010 **double bright band** event captured by vertically pointing radar, 915 MHz profiler, and ceilometer. The increase in the altitude of the **primary bright band** is due to the passage of a **warm front**. An **elevated melting layer** formed above a lower, preexisting melting layer closer to the surface. By 1744 UTC, the **secondary bright band** appeared at 2.9 km altitude following the surface warm front passage and warming of the entire layer below 2.9 km altitude to above 0°C. Continued warming of the lower atmosphere eventually erased the lower melting layer.



Name: Amber Emory, NASA/GSFC, Code 612

E-mail: amber.emory@nasa.gov

Phone: 301-614-6274

References:

Emory, A. E., B. Demoz, K. C. Vermeesch, and M. Hicks. 2014. "Double bright band observations with high-resolution vertically pointing radar, lidar, and profilers." *Journal of Geophysical Research: Atmospheres*. **119** (13): 8201-8211 [10.1002/2013JD020063]

Data Sources: EDOP is a coherent X band (9.6 GHz/3.123 cm) frequency radar that worked as a ground-based vertically pointing radar at NASA GSFC from 2007 until 2011. The radar measured the vertical evolution of the reflectivity, vertical velocity structure, and spectrum width with 0.5 s temporal and 37.5 m spatial resolution, which allowed a detailed evolution of the double bright band feature of this case to be captured. At the Howard University Beltsville site, the Maryland Department of the Environment (MDE) has a 915 MHz DeTect RAPTOR DBS-BL/LAP-3000 radar wind profiler that operates by transmitting electromagnetic energy vertically and in north-south and west-east vertical planes. The Doppler frequency shift of the backscattered energy retrieved from this transmission is then used to measure wind speed and direction. In addition, the MDE wind profiler and radio acoustic sounding system (RASS) combination measures wind profiles from the surface to approximately 4 km, depending on atmospheric aerosol loading, and virtual temperature profiles to approximately 2.5 km. The ceilometer used in this study is a Vaisala CT25K with a vertical range of 7 km and uses an eye-safe, class 1-pulsed Indium Gallium Arsenide diode laser at a wavelength of 905 nm with a 1.6 μ J pulse at 5 kHz. The profiler and ceilometer instruments are located at the Howard University Beltsville Research Campus (HUBRC), which is located 11 km from the NASA Goddard Space Flight Center (GSFC).

Technical Description of Figures:

Graphic 1: Profiles of radar reflectivity (top) and vertical velocity (bottom) during the warm front passage on 11 May 2010. Vertical lines mark the start (1719 UTC) and end (1735 UTC) of the double bright band feature. Below the bright band, complete melting occurred where fall speeds reached values greater than approximately 5 m/s, which is a typical value for small raindrops. Interestingly, with the start of the double bright band at approximately 1719 UTC on 11 May 2010, downward vertical velocity speeds failed to increase to 5 m/s below the elevated melting layer, which suggests that while some melting at the surface of frozen aggregates may have occurred to produce the first bright band at 2.9 km, refreezing likely occurred quick enough to keep hydrometeors from obtaining falling speeds more closely associated with liquid raindrops.

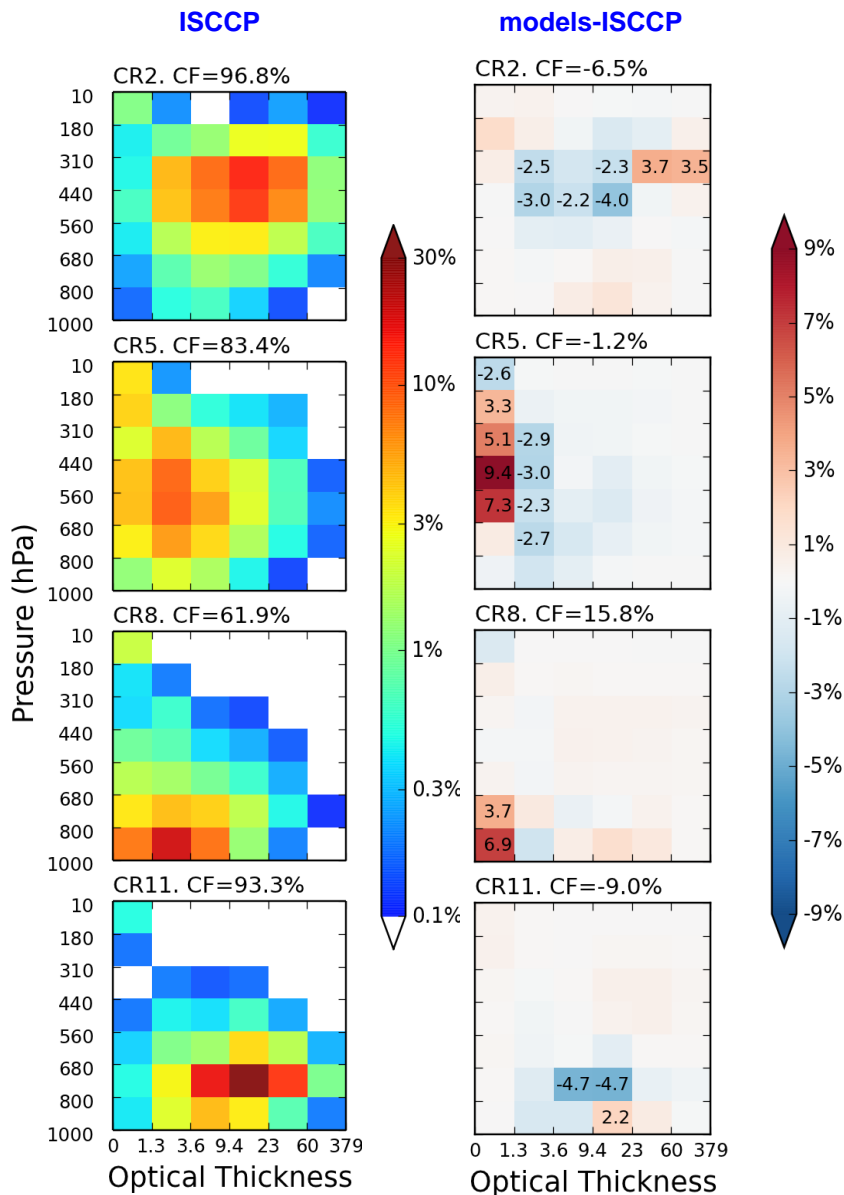
Graphic 2: Vertical temperature profiles from 1200 UTC 11 May 2010 and 0000 UTC 12 May 2010 soundings taken in Sterling, VA, with bright band altitudes determined from EDOP overlaid. The solid black line is the vertical temperature profile from the 1200 UTC 11 May 2010 sounding, the dashed black line is the vertical temperature profile from the 0000 UTC 12 May 2010 sounding, the red line is the height of the first bright band that appeared at 1.7 km, the blue line is the height of the second bright band that appeared at 2.9 km with the arrival of the warm front aloft before reaching the surface, and the vertical gray line marks the melting level. Based on the Doppler vertical velocities shown in **Graphic 1**, hydrometeors that melted below the higher bright band never refroze and continued to fall to the surface as liquid precipitation.

Scientific significance, societal relevance, and relationships to future missions: Although observations of double bright bands are somewhat rare, the ability to identify this phenomenon is important for rainfall estimation from spaceborne sensors, such as GPM, because algorithms employing the restriction of a radar bright band to a constant height, especially when sampling across frontal systems, will limit the ability to accurately estimate rainfall.

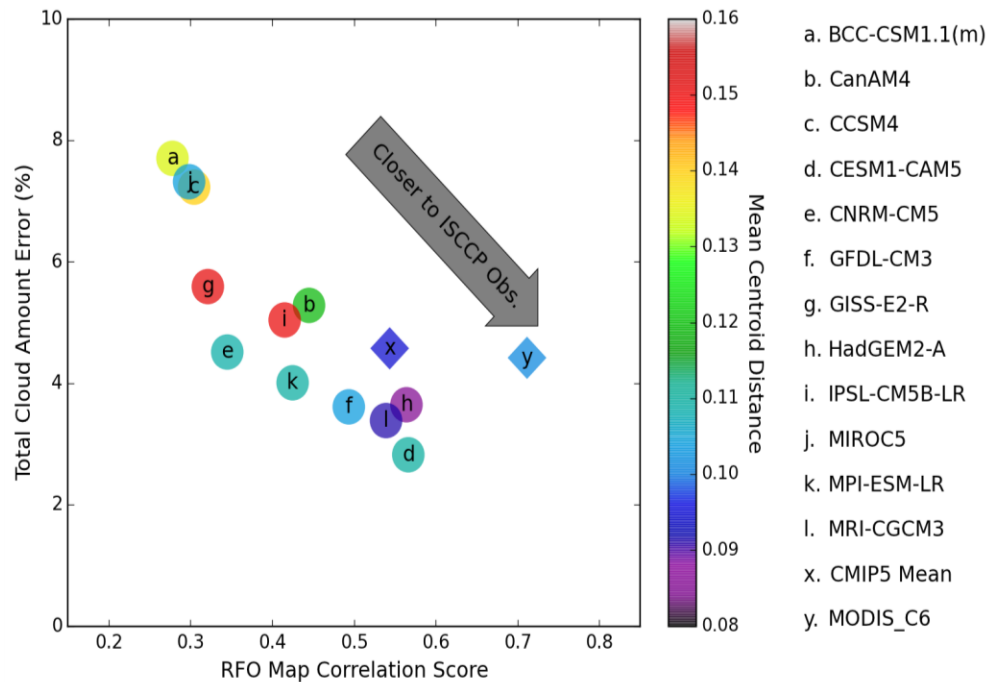


New ways to evaluate IPCC model cloudiness using ISCCP cloud regimes

Lazaros Oreopoulos, Daeho Jin, and Dongmin Lee (Code 613)



Select ISCCP cloud regimes (CRs, left) and comparison with IPCC multi-model mean (right)



Combination of three evaluation metrics to assess verisimilitude of clouds in IPCC GCMs (and MODIS) to ISCCP

We have developed a novel framework of detailed cloud evaluation for GCMs employing a satellite simulator of passive measurements. This framework allows us to distinguish clearly the IPCC GCMs that simulate better clouds.



Name: Lazaros Oreopoulos, NASA/GSFC, Code 613
E-mail: Lazaros.Oreopoulos@nasa.gov
Phone: 301-614-6128

References:

- Jin, Daeho, Lazaros Oreopoulos, and Dongmin Lee (2015), Regime-based Evaluation of Cloudiness in CMIP5 Models, *Climate Dynamics*, in review.
- Tselioudis G, Rossow W, Zhang Y, Konsta D (2013) Global Weather States and Their Properties from Passive and Active Satellite Cloud Retrievals. *Journal of Climate* 26:7734–7746. doi: 10.1175/JCLI-D-13-00024.1

Data Sources: We use the eleven (11) so-called ISCCP “global weather states” (we call them simply “cloud regimes”) of Tselioudis et al. (2013) obtained from *k-means* clustering analysis to the 42-element cloud fraction (CF) vectors formed from the joint (2D) histogram of cloud top pressure CTP and cloud optical thickness TAU in 3-hourly, equal area (280km × 280km) grid cells of ISCCP D1 data from July 1983 to December 2009. We also used Terra and Aqua daily histograms for 12 years starting December 2002, and the data was handled as if they were model data. Our analysis relies on the availability of ISCCP simulator outputs in phase 2 of the Cloud Feedback Model Intercomparison Project (CFMIP-2; <http://www.cfmip.net>), which is part of the fifth Coupled Model Intercomparison Project (CMIP5) used extensively in the last IPCC. Among the various scenarios explored in CMIP5, the Atmospheric Model Intercomparison Project (AMIP) run which uses prescribed sea surface temperatures is the most appropriate for our purposes. We use outputs from 12 models maintained and operated by 11 institutions. Each modeling group has archived daily mean ISCCP simulator outputs on the model’s own grid, subsequently interpolated (along with the ISCCP and MODIS data) to a common 2.5°, with a data timespan of ~30 years starting in January 1979.

Technical Description of Figures

Multipanel Graph: *Left panels:* Select (four out of eleven) cloud regime (CR) centroids of ISCCP joint CTP-TAU histograms per Tselioudis et al. (2013). The cloud fraction of each regime (sum of 42 bin CF values) is also provided. The CRs represent the dominant cloud mixtures around the globe as expressed by CTP-TAU co-variations. *Right panels:* CR centroid biases for the multi-model mean (CMIP5 Mean) with respect to observed ISCCP centroids. The panel legends provide cloud fraction (CF) difference from observed CR CF. By definition, the sum of the differences in the 42 individual bins is equal to this cloud fraction difference. When bin values are larger than 2% in absolute value, they are explicitly shown. Each CMIP5 GCM has its own version of CR centroid obtained by “forcing” each gridcell daytime joint histogram to the closest ISCCP CR and averaging all histograms belonging to the same CR (similarly for MODIS). The four panels provide an idea of the range of errors not only in total CF, but also in individual bin CFs. Small overall CF error (CR5) can be the result of large (but opposing) bin CF errors,

Graph with colored circles and diamonds: Composite plot of individual CMIP5 model performance *across all CRs* weighted by ISCCP Total Cloud Amount (TCA) which is the product of the CF of the previous graph and the CR relative frequency of occurrence (RFO). TCA Error is plotted against RFO map correlation with the color of the symbols indicating CR mean centroid Euclidean distance from the observational counterpart. Model (and MODIS) performance is best if the symbol is of purple hue (low mean distance from ISCCP centroid) and as close as possible to the bottom right corner of the plot (where TCA error is low and correlation score high). The three metrics in this plot allow us to basically check whether simulated clouds produce CRs that resemble the observed ones in the way CTP-TAU co-vary, have correct contributions to overall global cloudiness, and occur at the right locations.

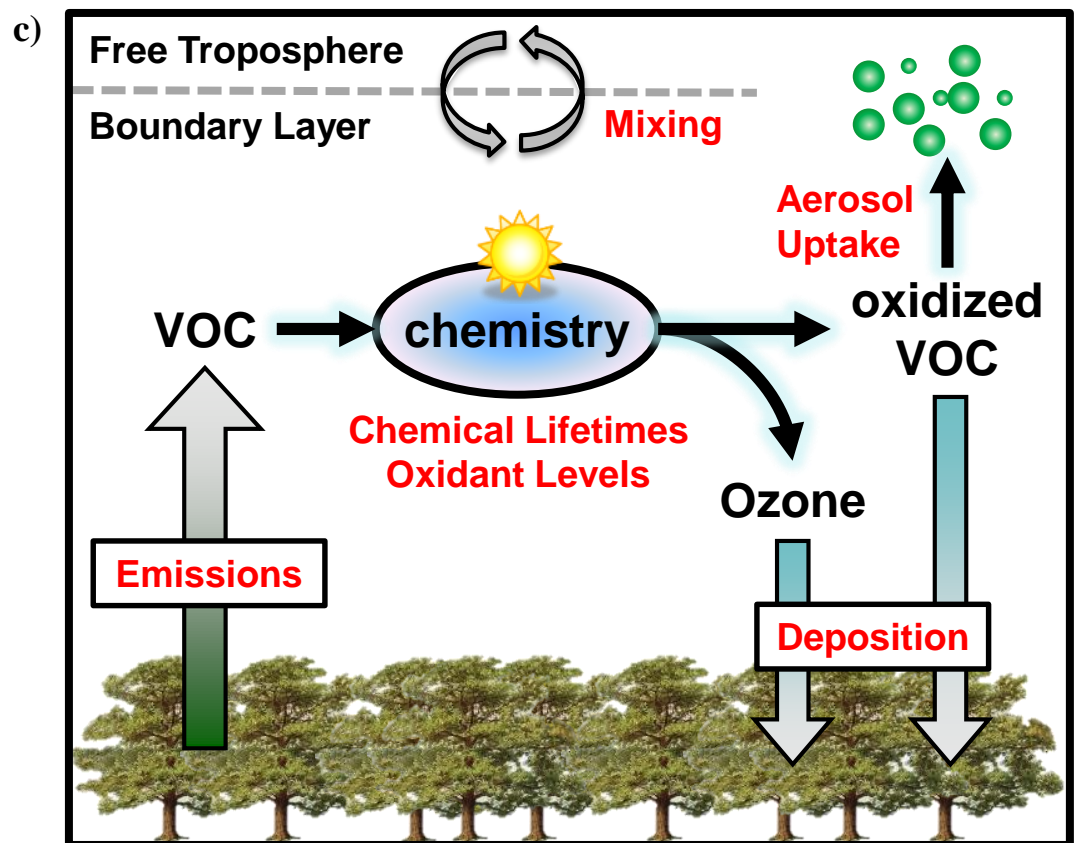
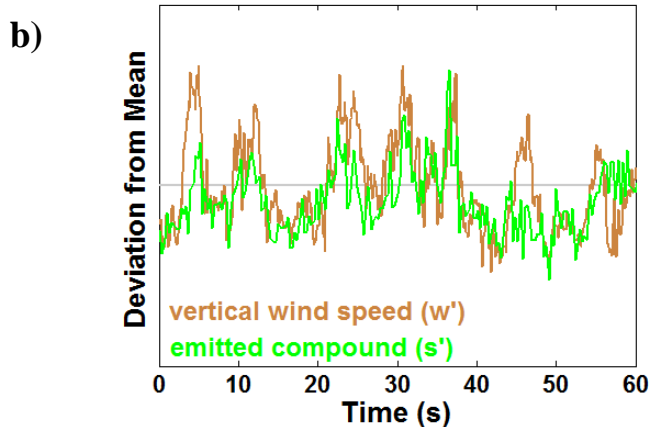
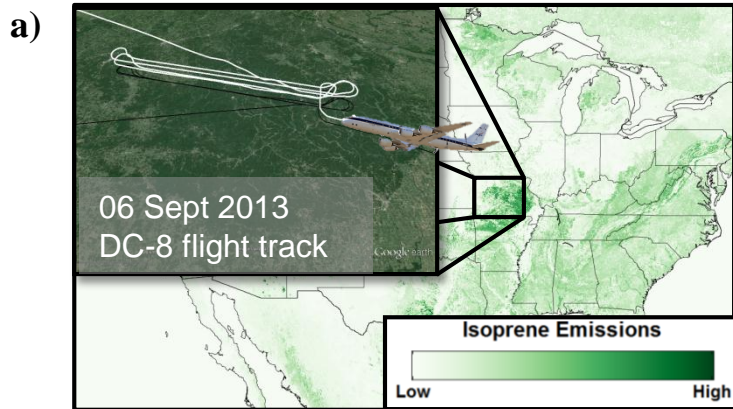
Scientific significance, societal relevance, and relationships to future missions: The primary goal of our work was to identify common deficiencies and strengths in CMIP5 cloudiness using an analysis that provides a different perspective on how a model fares compared to its peers. Replication with other observational datasets is possible, as long as output from appropriate satellite simulators is available. For example, our group has also derived global CRs from MODIS, and since this instrument’s simulator is also part of the COSP satellite simulator package, future intercomparison protocols should consider requiring this particular output. A revisit of the analysis shown in this paper with MODIS would allow us to determine the degree to which the major findings of the study reflect inherent model characteristics rather than idiosyncrasies of the particular observational dataset and simulator.



First Observations of Vertical Fluxes from the NASA DC-8 Directly Quantify Chemical Transformations and Surface-Atmosphere Exchange



In Situ Observations Laboratory, Code 614, NASA/GSFC and JCET/UMBC



Predictive capability requires understanding the fundamental *processes* that control atmospheric composition. During SEAC⁴RS, the NASA DC-8 flew over the Ozark Mountains, a hotspot for vegetative emissions of volatile organic compounds (VOC) that fuel production of ozone and aerosol. Vertical fluxes for a suite of reactive gases, derived from this novel dataset, provide *direct observational constraints* on the physical and chemical processes that impact air quality and climate.



Name: Glenn Wolfe, NASA/GSFC, Code 614 and JCET
E-mail: glenn.m.wolfe@nasa.gov
Phone: 301-614-6008



References:

Wolfe, G. M. (614/JCET), Hanisco, T. F. (614), Arkinson, H. L., Bui, T. P. Crouse, J. D., Dean-Day, J., Goldstein, A., Guenther, A., Hall, S. R., Huey, G., Jacob, D. J., Karl, T., Kim, P. S., Liu, X., Marvin, M. R., Mikoviny, T., Misztal, P. K., Nguyen, T. B., Peischl, J., Pollack, I., Ryerson, T., St. Clair, J. M. (614/JCET), Teng, A., Travis, K. R., Ullmann, K., Wennberg, P. O., Wisthaler, A., "Quantifying sources and sinks of reactive gases in the lower atmosphere using airborne flux observations," *Geophysical Research Letters*, 42, 8231-8240, 2015, doi: 10.1002/2015GL065839.

Data Sources: SEAC⁴RS (Studies of Emission and Atmospheric Composition, Clouds and Climate Coupling by Regional Surveys) observations available at DOI: 10.5067/Aircraft/SEAC4RS/Aerosol-TraceGas-Cloud. Isoprene emission factors are taken from MEGAN v2.1 emission inventory.

Technical Description of Figures:

a): Map of isoprene emission factors from the MEGAN v2.1 inventory. The inset shows the flight path (white line) and corresponding ground track (black line) for the 06 September 2013 SEAC⁴RS flight over the Ozark Mountains. The DC-8 entered from the east at ~13:10 local time and executed a series of four vertically-stacked legs (a "ladder" profile) along a 75 km east-west transect.

b): Simultaneous fast observations of vertical wind speed (w') and an emitted compound, isoprene (s'), for a 60-second portion of the flight pattern shown in a). The upward and downward motions of the atmosphere represent turbulence, driven by solar heating at the surface (think about steam rising from a cup of coffee). Isoprene concentrations are higher in the upward-moving air masses, indicating emissions. The product $w's'$ defines the eddy covariance flux, which is what we have quantified for numerous species.

c): Illustration of key processes in the forested convective boundary layer. Red text indicates parameters quantified via flux analysis. VOC = volatile organic compound.

Scientific significance, societal relevance, and relationships to future missions: Understanding the chemistry of the lowermost atmosphere requires knowledge of a wide range of chemical species, their interactions with one another, and how those interactions vary in different environments. To date, most observational efforts have focused on measuring the concentrations of the most important gases, but what we ultimately need to know for predictive capability is the *rates* of underlying processes – chemistry, emissions, deposition and transport. This study demonstrates the first-ever calculation of vertical fluxes from the DC-8, and furthermore shows how to use such data to build a picture of the boundary layer that is at once quantitative, comprehensive, and self-consistent. Fluxes offer a *direct observational constraint* on photochemistry and surface-atmosphere exchange – central drivers of variability in air quality and climate. On future airborne missions, airborne fluxes will allow us to link space-borne observations of atmospheric composition (including reactive compounds, greenhouse gases and aerosols) to the fundamental processes that control their abundance.